Evolution of ischemia and neovascularization in a murine model of full thickness human wound healing

Aos S. Karim, MD[1], **Aiping Liu, PhD**[1], **Christie Lin, PhD**[2,3], **Adam J. Uselmann, PhD**[2,3], **Kevin W. Eliceiri, PhD**[2,3,4], **Matthew E. Brown, PhD**[1], **Angela L. F. Gibson, MD, PhD**[1]

[1]Department of Surgery, University of Wisconsin School of Medicine and Public Health, Madison, Wisconsin

[2]OnLume Inc., Madison, Wisconsin

[3]Department of Medical Physics, University of Wisconsin-Madison, Madison, Wisconsin

[4]Department of Biomedical Engineering, University of Wisconsin-Madison, Madison, Wisconsin

Abstract

Translation of wound healing research is limited by the lack of an appropriate animal model, due to the anatomic and wound healing differences in animals and humans. Here, we characterize healing of grafted, full-thickness human skin in an in vivo model of wound healing. Full-thickness human skin, obtained from reconstructive operations, was grafted onto the dorsal flank of NOD.Cg-Kit^{W41J} $Tyr+$ $Prkdc^{scid}$ $Il2rg^{tm1Wjl}$/ThomJ mice. The xenografts were harvested 1 to 12 weeks after grafting, and histologic analyses were completed for viability, neovascularization, and hypoxia. Visual inspection of the xenograft shows drying and sloughing of the epidermis starting at week four. By week 12, the xenograft appears healed but has lost $63.05 \pm 0.24\%$ of the initial graft size. There is histologic evidence of epidermolysis as early as 2 weeks, which progresses until week 4, when new epidermis appears from the wound edges. Epidermal regeneration is complete by week 12, although the epidermis appears hypertrophied. An initial increase of infiltrating immune mouse cells into the xenograft normalizes to baseline 6 months after grafting. Neovascularization, as evidenced by positive staining for the proteins human CD31 and alpha smooth muscle actin, is present as early as 2 weeks after grafting at the interface between the xenograft and the mouse tissue. CD31 and alpha smooth muscle actin staining increased throughout the xenograft over the 12 weeks, leading to greater viability of the tissue. Likewise, there is increased Hypoxia Inducible Factor 1-alpha expression at the interface of viable and nonviable tissue, which suggest a hypoxia-driven process causing early graft loss. These findings illustrate human skin wound healing in an ischemic environment, providing a timeline for use of full thickness human skin after grafting in a murine model to study mechanisms underlying human skin wound healing.

1 | INTRODUCTION

Wound healing is a complex process that relies on several factors to proceed in an orderly fashion. First, the wound requires adequate vascular supply for delivery of nutrients and oxygenation.[1] Oxygen tension of the tissue is an important determinant of wound healing, as it is involved in several processes including collagen deposition, angiogenesis, and defense against infection through reactive oxygen species.[2] Second, wound healing requires an intact immune system.[3] The innate immune system, and more specifically macrophages, play an important role in facilitating wound healing. Furthermore, conditions that interfere with the immune system, such as steroid use, chronic inflammation, and infection can lead to dysfunctional wound healing.[3–5]

With an adequate vascular supply and an intact immune system, wound healing progresses by the infiltration of various cellular types. Immediately after wounding, a platelet plug is formed, which ensures hemostasis. This is followed by infiltration of neutrophils, which help fight infection and clear necrotic tissue.[5,6] In the next step, which takes several weeks, macrophages infiltrate the wound. These cells contribute to clearance of necrotic tissue, as well as tissue remodeling, which can occur over several months. In addition to inflammatory cells, epidermal stem cells (ESC) from the epidermal basal layer proliferate and migrate to achieve wound closure.[7] ESCs reside in the interfollicular epidermis, the epithelial basal layer lining the hair follicles, sebaceous glands, and sweat glands.[8]

The use of animal models to recapitulate human skin wound healing presents some challenges, due to differences in animal and human skin anatomy. Most current methods for studying wound healing in vivo use porcine or murine animal models. Porcine skin models are widely accepted as the best approximation for human skin wound healing (Table 1); however, porcine models are expensive and may vary significantly between breeds.[9,10] While rodent models are cheaper, can be easily genetically modified, and have a higher throughput, rodents are less ideal as a model because they heal primarily by wound contraction, whereas humans heal primarily by epithelialization.[7,11] These challenges highlight the need for a highthroughput model of human wound healing. One such model is an ex vivo human skin model.[12] While this organ model system contains all local components of human skin, such as hair follicles, sweat glands, capillaries, resident immune cells, and extracellular matrix, it lacks the systemic immune response associated with wound healing, which requires perfusion and oxygenation of the wound. To address these issues, human skin can be grafted on immunocompromised mice with minimal risk of graft rejection.[13]

Thus far, attempts to use human skin in wound healing studies have focused on the athymic mouse model (eg, FOXN1[nu/nu], BALB/c-nu) where the human xenograft can be transplanted onto the mouse and remains viable 1 year after transplant.[10,14–17] However, depending on the specific mouse strain used, rejection may still occur to varying degrees.[15,16] Even though the athymic mouse theoretically does not have adaptive T cell immunity and, therefore, cannot completely reject the grafts, studies have shown that this and other

similar immunocompromised strains can become "leaky," that is, still harbor a reduced but functional adaptive response, although the data for this are inconsistent.[18]

Here, we describe human skin grafting on the NBSGW (NOD.CgKit^{W-41J} Tyr$^+$ Prkdc^{scid} Il2rg^{tm1Wjl}/ThomJ) mouse strain. This immune-compromised murine model is advantageous because it lacks any known leakiness in the immune system and does not need to be irradiated like the NSG (NOD.SCID Il2rγ$^{-/-}$) mouse, which has been a staple in the study of function and pathophysiology of human diseases involving the immune system. Humanized mouse burn models have demonstrated mobilization of human inflammatory cells into burn wounds created on the skin of mice.[19] However, the fundamentally distinct wound healing mechanisms between rodents and humans make it difficult to draw conclusions from these models. By combining two well-established technologies, a mouse model capable of humanization and the ex vivo excisional skin model, into one unified model, we characterize full thickness skin wound healing in an in vivo system that can recapitulate healing in humans. Improved understanding of the mechanisms that underly wound healing will guide future studies in the use of technologies to enhance the regenerative capacity of wounds.

2 | MATERIALS AND METHODS

2.1 | Skin tissue retrieval and processing

De-identified, normal abdominal human skin was obtained from patients (n = 10) undergoing plastic reconstructive operations (abdominoplasty, panniculectomy, and deep inferior epigastric perforator flap reconstruction), using an Institutional Review Board exempt protocol in accordance with laws and regulations of the University of Wisconsin-Madison School of Medicine and Public Health. Tissue was kept on ice during transport. Prior to grafting, the tissue was rinsed with phosphate buffered saline (PBS) and 1×2 cm grafts were created using a scalpel. Subcutaneous fat was removed, and the grafts were placed in a culture dish that contained the growth medium RPMI (Gibco, 31800–014) on ice for transport to the animal procedure room.

2.2 | Animal surgery, care, and euthanasia

Human skin grafting onto the immunocompromised mouse has been previously described.[10,16,17,20] Briefly, animal use protocol approval was obtained from the University of Wisconsin Institutional Animal Care and Use Committee and the Research Animal Resource and Compliance office. Forty-three, 8- to 12-week-old male (53%) and female (47%) NBSGW mice (Humanized Mouse Core, University of Wisconsin, Madison, Wisconsin) were grafted in batches of four to five mice each.[21] Average mouse weight was 25 g at the time of grafting. Mice were anesthetized using isoflurane (Akorn, 59399–106-01) and maintained under anesthesia with isoflurane at ~3% with flow rate of 1.0 mL/min. Ocular ointment was added to prevent eye drying (Akorn, 59399–162-35). The dorsal flank was shaved using clippers, and the shaved area was cleansed using 2% chlorhexidine (Agrilabs, AL1040). A full thickness 2×1 cm skin wound was created using scissors. The human skin graft was sutured in place using 5–0 vicryl suture (Ethicon, J493G) in the four cardinal positions, taking care to include the underlying muscle to stabilize the graft to the mouse chest wall. Surgical glue (3M Vetbond, 1469SB) was used to approximate

gaping areas of the wound. The wound was covered with a thin layer of petroleum jelly and Cuticerin (Smith and Nephew, 66045503). The wound was then covered with an elastic adhesive bandage circumferentially (BSN Tensoplast, 02139–00) and secured with a surgical stapler (Ethicon, PXR35). Mice were injected with 0.05 to 0.10 mg/kg of buprenorphine (PAR Pharmaceuticals, 42023–179-05) diluted to 0.015 mg/mL. At the end of the procedure, mice were awakened from anesthesia and monitored daily for the next 3 days for signs of distress. Bandages were changed weekly under anesthesia for 4 weeks. Xenografts were left open to air at 4 weeks after grafting until time of sacrifice. At the time of sacrifice, mice were euthanized using carbon dioxide asphyxiation. The xenografts were excised with a rim of normal mouse skin. After bisecting the xenografts, one half of the tissue was fixed in 10% neutral buffered formalin (Sigma, HT501128–4L) prior to paraffin embedding, while the other half was washed with PBS and oriented in Tissue-Tek OCT Compound (Sakura FineTek, 4583), then frozen using a cold metal block.

2.3 | Histology and image analysis

Eight-micron thick frozen and five-micron thick paraffin sections were prepared. Paraffin samples were stained for H&E, human cluster of differentiation 31 (CD31, Abcam, ab76533, 1:400), alpha-smooth muscle actin (α-SMA, Sigma, A2547, 1:5000), human mitochondrial (Sigma, MABt1273, 1:1500) and hypoxia inducible factor 1-alpha (HIF-1α, Lifespan Biosciences, LS-B495, 1:300). Primary antibodies were incubated overnight at 4°C. Secondary antibodies (Vector Labs, anti-rabbit: MP5401, anti-mouse: MP5402) were incubated for 35 minutes at room temperature. DAB (Vector Labs, SK-4105) was applied to the sections for 2 minutes at room temperature, then sections were counterstained in Harris hematoxylin for 2 minutes. Frozen samples were stained for lactate dehydrogenase (LDH) as previously described.[22] Tissue sections were viewed using a Nikon Ti-S inverted microscope and digital images were captured with Nikon DS Ri2 cooled color camera, X-Cite 120LED BOOST System lamp from Excelitas, and Nikon Imaging Software, NIS Elements (Nikon, Tokyo, Japan). Bright field images were taken at 40 to 400× magnification.

2.4 | Quantification of epidermal thickness

Epidermal thickness was measured in an unblinded fashion using Nikon NIS software. Ten to twenty measurements, 100 μm apart, were taken along the entire width of skin sample.

2.5 | Semi-quantification of cellular infiltrate

Automated semi-quantification of cellular counts have been previously described.[23,24] For grafted skin tissue, five random high-power field (400×) images were taken at the interface between human and mouse tissue to standardize the measurement of cellular infiltrate. For ungrafted skin tissue, five random high-power field pictures were taken anywhere along the graft. Cells were counted using a batch analysis macro developed in Fiji.[25] Briefly, the images were separated into red, blue, green channels using the plugin "Colour deconvolution" in Fiji and the "H&E" algorithm. The blue channel was selected because nuclei stain blue on H&E, and the image threshold plugin was applied using the "MaxEntropy" algorithm. The "Despeckle" and "Watershed" algorithms were run to remove noise artifact and separate nuclei that overly each other for more accurate counts. Finally, the "Analyze Particles" module was applied with the following parameters: Circularity

0.50–1.00, size: 50 - infinity pixels. Outlines of the counted cells were visualized, and all images were reviewed for quality control to make sure that we captured the majority of cells. Overall, the algorithm is conservative and slightly underestimates the number of cells (Supplementary Figure 1).

2.6 | Fluorescence microangiography

Cardiogreen (Indocyanine green, Sigma, 21980–100 mg-F) powder was resuspended using sterile water in accordance with manufacturer recommendations at 1 mg/mL, vortexed until dissolved, sterile filtered, then diluted to a concentration of 0.3 mg/mL using sterile PBS. At 4 and 12 weeks post grafting, mice were anesthetized using isoflurane as previously described, then injected intravenously with indocyanine green at a concentration of 1 mg/kg in the retro-orbital space. Images were captured immediately following injection using the OnLume small animal fluorescence imaging system (Onlume Inc, Madison, Wisconsin).

2.7 | Blood collection and flow cytometry

For each sample, 300 μL of a 50:50 solution of 2% Dextran and Novaplus sodium heparin was prepared. Mice were anesthetized and bled from the retro-orbital space using heparinized microcapillary tubes, and the tube was placed in the 50:50 solution prepared earlier. After blood was allowed to separate for 30 minutes, the upper layer containing white blood cells was moved to a new tube. The cells underwent further cleaning using 1000 μL of PBS at 400× RCF for 7 minutes, 500 μL of ACK buffer at 400× RCF for 7 minutes, 500 μL of FACS buffer for 7 minutes at 400× RCF (×2), then 1000 μL of FACS buffer at 4000× g for 7 minutes. Supernatant was removed between steps. After the final cleaning step, the supernatant was decanted, and the cell pellet resuspended in the remaining fluid in the tube. Mouse samples were stained with APC Mouse antihuman CD45 (BD, 555485) and FITC rat anti-mouse CD45 (BD, 553080). FITC-rat IgG2b (BD, 553988) and APC-mouse IgG (BD, 555751) served as isotype controls.

2.8 | Statistical analysis

All statistical analyses were performed using Graphpad Prism version 8 for Windows (Graphpad, La Jolla, California). Mean and SE of the mean values are presented as X ± Y. Error bars in figures show SE of the mean. Level of significance was determined at P 0.05.

3 | RESULTS

3.1 | Gross evaluation of xenografts

Grafted NBSGW mice were imaged weekly for 12 weeks to monitor healing of the xenograft (Figure 1A). All mice had graft take, and all except one mouse lived until the time they were sacrificed. The one mouse that died prematurely at week 9 after grafting had an intact graft at the time of death and the grafting did not appear to be the cause of death. Early visualization of the xenograft revealed gross viability for the first 2 weeks. At 3 weeks, some signs of epidermal stress could be seen, but overall, the xenograft appeared viable on visual inspection and was adhered to the wound bed. After 4 weeks, when bandages were removed and the xenograft was left open to air, the edges of the xenograft appeared to be

desiccating and flaking, suggesting full loss of the epidermis. Between weeks 5 to 8, there was continued desiccation and sloughing of the epidermal layer, with gradual increase in a rim of hypertrophic tissue at the edges of the xenograft. By 8 to 9 weeks there was minimal desiccated epidermal tissue remaining, and by 10 to 12 weeks the xenografts appeared completely reepithelialized. By 12 weeks, the xenograft also flattened and became less pink. The overall area of the remaining xenograft by 12 weeks was reduced by $63.05 \pm 0.24\%$ from the original xenograft size (Figure 1B).

3.2 | Viability evaluation of xenografts

Explanted human skin is viable for several days at 37°C and even longer at 4°C.[26] In our study, full thickness biopsy of the xenograft 1 week after grafting shows viable epidermal and dermal cells, as evidenced by staining for LDH throughout the tissue (Figure 2B) similar to the viability of the tissue on the day of grafting (Figure 2A). Despite the normal gross appearance of the xenograft throughout the first 2 weeks, histologic evidence of cell death is present in the upper dermis and entire epidermis as early as 2 weeks post grafting; by week 4, most of the epidermis is shed (Figure 2C,D). Starting at 4 weeks, a rim of new epidermis is observed, which appeared to grow from the edges of the xenograft toward the center of the wound. At 3 months, xenografts are completely healed with restoration of the epidermis and formation of Rete ridges (Figure 2F). The effects of grafting on the dermis, which is sparsely populated with cells at baseline, are not as apparent until 2 weeks when there is a loss of viability down to the mid-dermal region. The cellular viability is present throughout the dermis again by week 8 (Figure 2E), however, it has much greater density than baseline (Figure 2A). Finally, to confirm that the xenografts healed with human cells rather than mouse cells, we stained the explanted xenografts with a human mitochondrial marker (Figure 3). A transition zone between the human skin graft and mouse skin is visible (Figure 3E), with the central portion of the healed graft consisting entirely of human dermal and epidermal cells (Figure 3F). The interface between mouse and human tissue was a chimerism of mouse keratinocytes on human dermis, suggesting that mouse keratinocytes migrated from the edge of the wound to repopulate the human dermal scaffold before it was fully revascularized.

3.3 | Full thickness grafts heal with epidermal hyperproliferation and dermal hypertrophy

Several studies have shown that grafting human skin onto an immune-compromised mouse leads to hypertrophic scarring.[14,15,20] Hypertrophic scarring, most often thought of as a dermal process, also receives input from the neighboring epidermis.[27,28] Compared to normal human skin, the epidermal thickness of xenografts was increased 1 to 6 months after grafting (Figure 4). Total dermal thickness was not measured due to variations in starting thickness of tissue from multiple individuals, and processing effects (uneven tissue compression) that occur in the dermis due to fixation and sectioning. Dermal hypertrophy was visualized grossly and accompanied the epidermal changes that were observed over time.

A cohort of mice grafted with either partial thickness or full thickness grafts (n = 1 full thickness and n = 2 partial thickness) exhibited similar epidermal thicknesses (143.49 ± 9.62 μm) at 6 months after grafting, despite differences in the initial xenograft thickness. While

there seems to be a trend toward a normalization in graft epidermal thickness, all grafted skin was significantly thicker than the normal skin (Figure 4).

3.4 | Xenografts exhibit sustained cellular infiltrate for months

The innate immune system plays a pivotal role in wound healing, and cellular infiltration by immune cells defines the stage of healing, with an increase of cells during healing and a normalization later during remodeling. Our observations are consistent with this timeline, as xenografts become infiltrated with cells within the first month and have a sustained, elevated cellular response up to the 3-month time point (Figure 5) when the repair from the ischemic insult is completed. The density of cellular infiltrate reverts to baseline within 6 months after grafting. H&E staining reveals that the infiltrate appears to be composed of neutrophils and monocytes. Given the lack of a human immune system, these cells are most likely mouse in origin. Flow cytometry performed on blood 6 months after grafting showed human CD45+ count of $0.63 \pm 0.25\%$, which is likely background noise and is not indicative of humanization of the mouse from resident human tissue leukocytes.

3.5 | Early graft loss is a hypoxia-mediated event

While cell-mediated rejection has been suggested to play a role in graft loss after full thickness grafting of human skin onto athymic mice,[16] an alternative explanation for the initial loss and then recovery of full thickness human skin xenografts is an ischemia and hypoxia-mediated mechanism. Staining of the human skin xenografts show minimal human CD31 (Figure 6A–D) and α-SMA (Figure 6E–H) staining within the graft at 2 weeks. By 4 weeks, there is a visible increase in expression of CD31 and α-SMA emanating from the edge of the xenograft abutting the mouse tissue. Neovascularization continues into the xenograft over time, and the xenograft is fully revascularized at 12 weeks post grafting. Furthermore, HIF-1α signaling was strongest at the edge of devascularized tissue in the earlier weeks and began to normalize as the graft healed, albeit not completely by week 12 (Figure 6I–L). Of note, HIF-1α was seen throughout the epidermis at baseline and after reepithelialization.

3.6 | Indocyanine Green microangiography correlates with histologic phenotype

To confirm the histologic findings of neovascularization, intravenous indocyanine green (ICG) was used to measure perfusion of the xenograft at the point of maximal damage at 4 weeks and the point of healing at 12 weeks (Figure 7). ICG is an FDA-approved dye used to visualize ischemic areas in plastic and reconstructive operations.[29] At 4 weeks after grafting, increased ICG fluorescence signal was observed at the periphery of the xenograft, while the center of the xenograft was devoid of ICG fluorescence (Figure 7B). Consistent with the histologic staining, which showed complete revascularization at 12 weeks (Figure 6D), the xenograft exhibited fluorescence signal throughout the graft (Figure 7D).

4 | DISCUSSION

In this study we follow the gross and histologic changes in grafted human skin as it heals from an ischemic insult in a model of full thickness human skin wound healing, using the NBSGW mouse. While other investigators have described full thickness human skin

healing on the athymic mouse, this model has been abandoned in favor of transplantation of partial thickness skin.[6,14,20,30,31] Partial thickness skin is often chosen over full thickness skin because it heals faster (generally within 7 weeks in our experience; unpublished data); the thinner dermal component revascularizes more rapidly, therefore, the model is ready for experimentation sooner than full thickness skin. However, full thickness skin better recapitulates the complete composition of human skin. Studies have shown that deep dermal tissue possesses a cellular complement that may be different from the superficial dermis.[14,20] Dunkin et al have shown that wounds deeper than 0.56 mm at the lateral thigh lead to hypertrophic scarring, which they postulated to be a response by a population of deep dermal fibroblasts, which secrete factors that predispose the healing wound to fibrosis and contracture.[32] In the context of burn wounds, there is a clinically important difference between superficial and deep dermal burns: superficial burns heal without surgery due to the presence of a greater density of epidermal progenitors located in the dermal skin appendages, whereas deep dermal and full thickness burns require excision and grafting for normal wound healing.[33] For this reason, the use of a full thickness grafting model, as we have shown, is important in the study of human burn wound healing.

In our experience, it takes 12 weeks for full thickness human skin grafts to shed the ischemic scab and resemble normal human skin grossly. This is in contrast to some other models that describe wound healing between 4 and 8 weeks after grafting.[15,30,34] This observation could not be explained by differences in the NBSGW mouse strain we used. Shanmugam et al used FOXN1[nu/nu] and it took their model a minimum of 12 weeks to heal, similar to our model.[10] Additionally, we have grafted nude mice (FOXN1[nu/nu]) with full thickness human skin using the same methodology employed for the NBSGW mice and we found the healing timeline to be consistent (Supplementary Figure 2). In this study, we follow the trajectory of wound healing while providing histologic evidence for recovery of the xenograft from the ischemic event of grafting. While other investigators claim that their grafts are fully healed within 4 to 8 weeks, they do not provide a definition of what that entails.

Yang et al, describe a model of full thickness skin grafting in athymic mice (BALB/c-nu), and speculated that early grafts are lost due to a process that resembled rejection.[16] Shanmugam et al also describe a possibility for rejection as well.[10] Even though rejection is mainly mediated by T and B lymphocytes, Yang et al suggested that mechanisms involving Natural Killer (NK) cells may be at play, as these cells are still present in athymic mice but not in other strains, such as the NBSGW used in our study. This conclusion is not surprising, given the monocellular infiltration of the xenograft as well as graft desiccation and loss of epidermis.[35,36] In our study, however, we suggest the involvement of an alternative process. While previous models are based on the athymic mouse, where there is evidence of leakiness in the adaptive immune system,[18] the NBSGW mice used in our study are deficient in T, B and NK cells due to the IL2rg mutation, and therefore unable to mount murine cell mediated allograft rejection.[13,37] We show that early graft loss in our model is likely hypoxia-mediated and is resolved after xenografts are revascularized. This is evident by the presence of HIF-1α at the edge of hypoxic tissue and the reemergence of epidermis and dermal viability in the areas where human CD31 and α-SMA staining is seen. The demonstrated early loss of epidermis is likely related to epidermolysis, which is caused by tissue hypoxia during the transition of inosculation to neovascularization of the xenograft.

Epidermolysis has been shown to take about 15 days to develop in uncultured, stored, ex vivo tissue as well as in vivo in rats.[26,38] It has been clinically observed after grafting of full thickness skin in humans. While initially unexpected, the degree of cellular infiltrate in the graft is consistent with the wound healing process, as the xenograft is severely damaged from the ischemic insult by 4 weeks after grafting, and undergoes extensive regeneration of necrotic tissue by human cells.[20] One study showed that treatment with Anti-GR1 antibody reduced this infiltrate and protected blood vessels from destruction, which may have accelerated wound healing.[39] In our experience, human CD31 staining reveals complete revascularization of the xenograft at 12 weeks. Further, fluorescence imaging of ICG confirms the patency of these vessels, and adequate perfusion in xenografts that still had murine cellular infiltrate throughout the tissue, as shown histologically. While the end goal of our study was to develop the mouse model for wound healing studies of full thickness wounds, we suggest the additional potential in our model to study ischemia in wound healing. Ischemic wounds such as those seen in diabetics foot ulcers and patients with peripheral vascular disease can be studied using the earlier timepoints of this model to test wound healing strategies and therapeutics that promote vascular regeneration.

While our model is promising for burn wound healing studies, as well as a number of other wound healing applications, there are limitations of our study that should be noted. First, we obtained deidentified tissue for our studies from individuals undergoing reconstructive operations, therefore, we are unable to determine if underlying disease, such as cancer and metabolic syndromes, may have introduced variability in the quality of skin grafted. Second, skin thickness was not measured prior to grafting or after sacrifice, leading to challenges in assessment of dermal hypertrophic scarring quantitatively. However, on gross assessment, all xenografts healed with a raised appearance, likely related to hypertrophic scarring. Finally, for the purpose of this study we aimed to determine the minimum amount of time that is needed for reepithelization of the graft, which we determined to be 3 months grossly and on histologic evaluation. On histology, we also noted that the xenografts have high cellularity throughout the tissue, suggesting that the xenografts may not have reached homeostatic equilibrium at that time. We report findings from three mice that we followed for 6 months, and we show that there is a dramatic decrease in the cellularity of the xenografts between the 3 and 6 months timepoints which are not captured by this study. These changes will be of interest to define in future studies.

In conclusion, the longitudinal characteristics of a full thickness, human skin xenograft healing were elucidated using an immunocompromised mouse strain. The xenografts require a minimum of 12 weeks to be considered fully engrafted and revascularized. Early graft loss appears to be related to hypoxia and lack of adequate nutritional support, which is mitigated when the graft undergoes full neovascularization. The NBSGW mouse used in this study is particularly well-suited for creation of human immune system humanized mice, via engraftment of human hematopoietic cell populations.[40] In future studies, we plan to humanize our model to get a more complete picture of burn wound healing in the context of the human adaptive immune system. There will be several considerations for this next step, as those studies will define the source of the immune cells (skinderived vs peripheral blood cells), the effect of humanization on wound healing and revascularization, and finally the timing of human immune cell engraftment post-skin graft in the context of development

of graft vs host disease. These studies will allow the study of the human immune response in the wound microenvironment. Our versatile model system can be used to study acute and chronic wound healing with recapitulation of the structure and function of human skin.

Supplementary Material

Refer to Web version on PubMed Central for supplementary material.

ACKNOWLEDGMENTS

Abbreviations:

CD31	cluster of differentiation 31
CD45	cluster of differentiation 45
H&E	hematoxylin and eosin
HIF-1α	hypoxia inducible factor 1 alpha
ICG	indocyanine green
IL2rg	interleukin 2 receptor subunit G
Kit	proto-oncogene receptor tyrosine kinase
LDH	lactate dehydrogenase
NBSGW	NOD.Cg-KitW−41J Tyr+ Prkdcscid Il2rgtm1Wjl/ThomJ
NK	natural killer cell
NOD	non-obese diabetic
Prkdc	protein kinase, DNA-activated, catalytic subunit
Scid	severe combined immunodeficiency
Tyr	tyrosinase
α-SMA	alpha smooth muscle actin

REFERENCES

1. Sen CK. Wound healing essentials: let there be oxygen. Wound Repair Regen. 2009;17(1):1–18. [PubMed: 19152646]

2. Castilla DM, Liu ZJ, Velazquez OC. Oxygen: implications for wound healing. Adv Wound Care (New Rochelle). 2012;1(6):225–230. [PubMed: 24527310]

3. Raje N, Dinakar C. Overview of immunodeficiency disorders. Immunol Allergy Clin North Am. 2015;35(4):599–623. [PubMed: 26454309]

4. Singh S, Young A, McNaught C-E. The physiology of wound healing. Surgery (Oxford). 2017;35(9):473–477.

5. Wynn TA, Vannella KM. Macrophages in tissue repair, regeneration, and fibrosis. Immunity. 2016;44(3):450–462. [PubMed: 26982353]

6. Tredget EE, Levi B, Donelan MB. Biology and principles of scar management and burn reconstruction. Surg Clin North Am. 2014;94(4): 793–815. [PubMed: 25085089]

7. Pastar I, Stojadinovic O, Yin NC, et al. Epithelialization in wound healing: a comprehensive review. Adv Wound Care (New Rochelle). 2014;3(7):445–464. [PubMed: 25032064]

8. Rittie L, Sachs DL, Orringer JS, Voorhees JJ, Fisher GJ. Eccrine sweat glands are major contributors to reepithelialization of human wounds. Am J Pathol. 2013;182(1):163–171. [PubMed: 23159944]

9. Seo BF, Lee JY, Jung SN. Models of abnormal scarring. Biomed Res Int. 2013;2013:423147.

10. Shanmugam VK, Tassi E, Schmidt MO, et al. Utility of a human-mouse xenograft model and in vivo near-infrared fluorescent imaging for studying wound healing. Int Wound J. 2015;12(6):699–705. [PubMed: 24373153]

11. Boyko TV, Longaker MT, Yang GP. Laboratory models for the study of Normal and pathologic wound healing. Plast Reconstr Surg. 2017; 139(3):654–662. [PubMed: 28234843]

12. Stojadinovic O, Tomic-Canic M. Human ex vivo wound healing model. Methods Mol Biol. 2013;1037:255–264. [PubMed: 24029940]

13. McIntosh BE, Brown ME. No irradiation required: the future of humanized immune system modeling in murine hosts. Chimerism. 2015;6(1–2):40–45. [PubMed: 27171577]

14. Ding J, Tredget EE. Transplanting human skin grafts onto nude mice to model skin scars. Methods Mol Biol. 2017;1627:65–80. [PubMed: 28836195]

15. Momtazi M, Ding J, Kwan P, et al. Morphologic and histologic comparison of hypertrophic scar in nude mice, T-cell receptor, and recombination activating gene knockout mice. Plast Reconstr Surg. 2015; 136(6):1192–1204. [PubMed: 26595016]

16. Yang DY, Li SR, Wu JL, et al. Establishment of a hypertrophic scar model by transplanting full-thickness human skin grafts onto the backs of nude mice. Plast Reconstr Surg. 2007;119(1):104–109; discussion 110–101. [PubMed: 17255662]

17. Berking C, Herlyn M. Experimental induction of human atypical melanocytic lesions and melanoma in ultraviolet-irradiated human skin grafted to immunodeficient mice. Methods Mol Med. 2001;61:71–84. [PubMed: 22323252]

18. Bosma GC, Fried M, Custer RP, Carroll A, Gibson DM, Bosma MJ. Evidence of functional lymphocytes in some (leaky) scid mice. J Exp Med. 1988;167(3):1016–1033. [PubMed: 3280724]

19. Costantini TW, Meads M, Dang X, et al. The response to burn injury in mice with human Hematolymphoid systems. Ann Surg. 2016;263 (1):199–204. [PubMed: 25575256]

20. Alrobaiea SM, Ding J, Ma Z, Tredget EE. A novel nude mouse model of hypertrophic scarring using scratched full thickness human skin grafts. Adv Wound Care (New Rochelle). 2016;5(7):299–313. [PubMed: 27366591]

21. McIntosh BE, Brown ME, Duffin BM, et al. Nonirradiated NOD,B6. SCID Il2rγ–/–kit(W41/W41) (NBSGW) mice support multilineage engraftment of human hematopoietic cells. Stem Cell Reports. 2015;4 (2):171–180. [PubMed: 25601207]

22. Gibson ALF, Shatadal S. A simple and improved method to determine cell viability in burn-injured tissue. J Surg Res. 2017;215:83–87. [PubMed: 28688666]

23. Grishagin IV. Automatic cell counting with ImageJ. Anal Biochem. 2015;473:63–65. [PubMed: 25542972]

24. Vayrynen JP, Vornanen JO, Sajanti S, Bohm JP, Tuomisto A, Makinen MJ. An improved image analysis method for cell counting lends credibility to the prognostic significance of T cells in colorectal cancer. Virchows Arch. 2012;460(5):455–465. [PubMed: 22527018]

25. Schindelin J, Arganda-Carreras I, Frise E, et al. Fiji: an open-source platform for biological-image analysis. Nat Methods. 2012;9(7): 676–682. [PubMed: 22743772]

26. Castagnoli C, Alotto D, Cambieri I, et al. Evaluation of donor skin viability: fresh and cryopreserved skin using tetrazolioum salt assay. Burns. 2003;29(8):759–767. [PubMed: 14636749]

27. Mustoe TA, Gurjala A. The role of the epidermis and the mechanism of action of occlusive dressings in scarring. Wound Repair Regen. 2011;19(Suppl 1):s16–s21. [PubMed: 21793961]

28. Andriessen MP, Niessen FB, Van de Kerkhof PC, Schalkwijk J. Hypertrophic scarring is associated with epidermal abnormalities: an immunohistochemical study. J Pathol. 1998;186(2):192–200. [PubMed: 9924436]

29. Gurtner GC, Jones GE, Neligan PC, et al. Intraoperative laser angiography using the SPY system: review of the literature and recommendations for use. Ann Surg Innov Res. 2013;7(1):1. [PubMed: 23289664]

30. Maldonado AA, Cristóbal L, Martín-López J, Mallén M, GarcíaHonduvilla N, Buján J. A novel model of human skin pressure ulcers in mice. PLoS One. 2014;9(10):e109003.

31. Ding J, Ma Z, Liu H, et al. The therapeutic potential of a C-X-C chemokine receptor type 4 (CXCR-4) antagonist on hypertrophic scarring in vivo. Wound Repair Regen. 2014;22(5):622–630. [PubMed: 25139227]

32. Dunkin CS, Pleat JM, Gillespie PH, Tyler MP, Roberts AH, McGrouther DA. Scarring occurs at a critical depth of skin injury: precise measurement in a graduated dermal scratch in human volunteers. Plast Reconstr Surg. 2007;119(6):1722–1732; discussion 1733–1724. [PubMed: 17440346]

33. Heimbach D, Engrav L, Grube B, Marvin J. Burn depth: a review. World J Surg. 1992;16(1):10–15. [PubMed: 1290249]

34. Berking C, Takemoto R, Binder RL, et al. Photocarcinogenesis in human adult skin grafts. Carcinogenesis. 2002;23(1):181–187. [PubMed: 11756239]

35. Vural E, Berbée M, Acott A, Blagg R, Fan CY, Hauer-Jensen M. Skin graft take rates, granulation, and epithelialization: dependence on myeloid cell hypoxia-inducible factor 1alpha. Arch Otolaryngol Head Neck Surg. 2010;136(7):720–723. [PubMed: 20644069]

36. Leibovitch I, Huilgol SC, Hsuan JD, Selva D. Incidence of host site complications in periocular full thickness skin grafts. Br J Ophthalmol. 2005;89(2):219–222. [PubMed: 15665356]

37. Zumwalde NA, Gumperz JE. Modeling human antitumor responses in vivo using umbilical cord blood-engrafted mice. Front Immunol. 2018;9:54. [PubMed: 29434589]

38. Richter GT, Bowen T, Boerma M, Fan CY, Hauer-Jensen M, Vural E. Impact of vascular endothelial growth factor on skin graft survival in irradiated rats. Arch Facial Plast Surg. 2009;11(2):110–113. [PubMed: 19289683]

39. Racki WJ, Covassin L, Brehm M, et al. NOD-scid IL2rgamma(null) mouse model of human skin transplantation and allograft rejection. Transplantation. 2010;89(5):527–536. [PubMed: 20134397]

40. Brown ME, Zhou Y, McIntosh BE, et al. A humanized mouse model generated using surplus neonatal tissue. Stem Cell Reports. 2018;10 (4):1175–1183. [PubMed: 29576539]
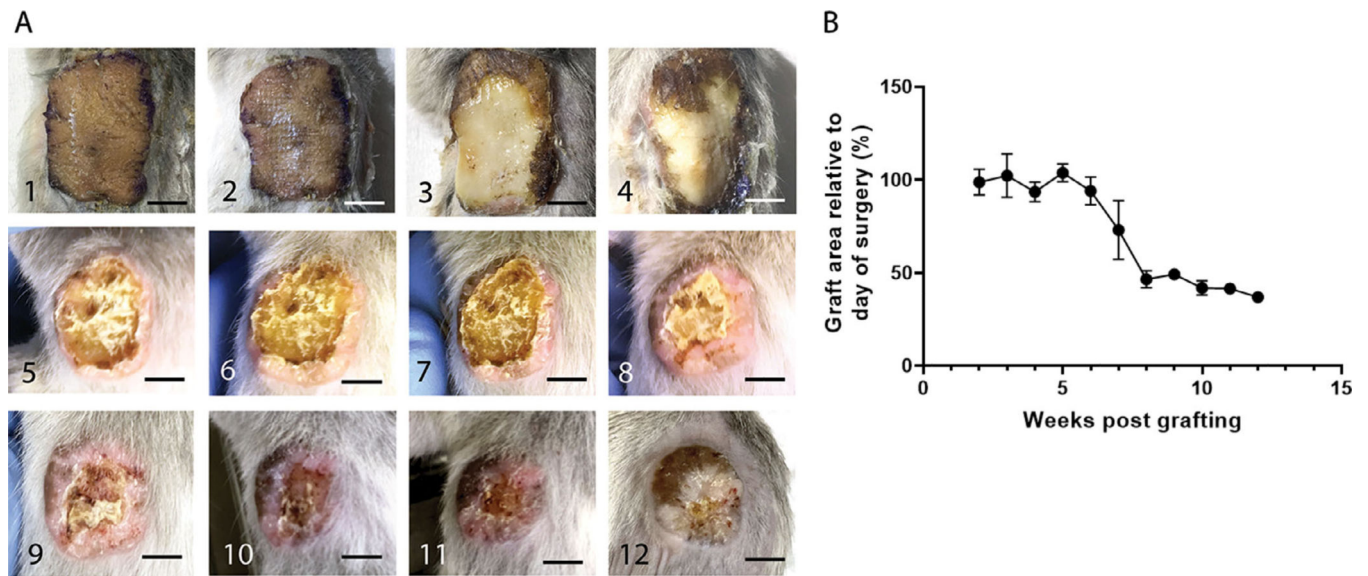
FIGURE 1. Full thickness human skin grafts undergo epidermolysis and contract by 65% relative to their original size 12 weeks after grafting.
A, 1–12, Weekly gross evaluation of one representative mouse from weeks 1 through 12. B, Quantification of the graft area relative to the day of surgery at 2 to 12 weeks post grafting (representative quantification of six animals per timepoint). Scale bars: 500 μm
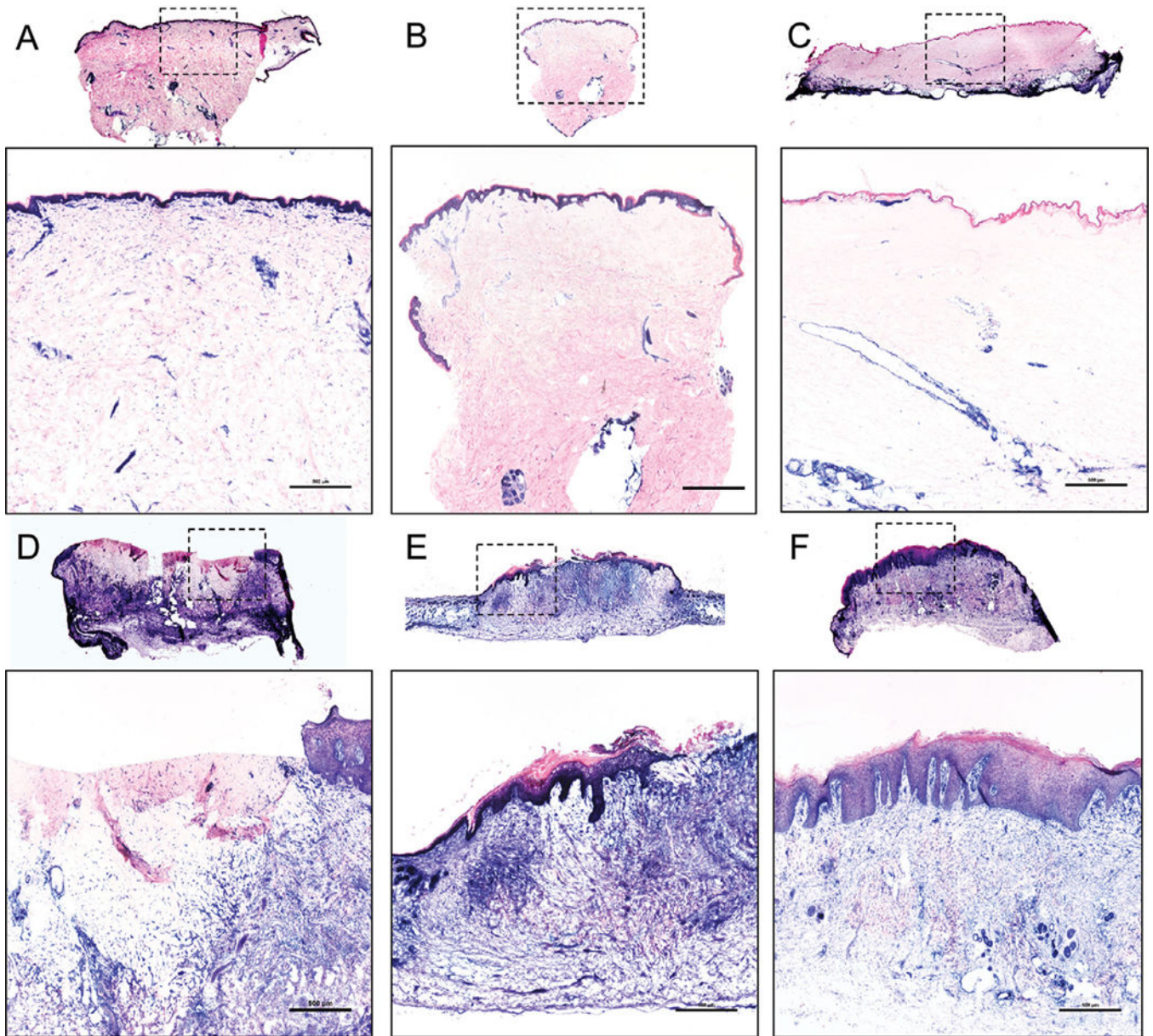
FIGURE 2. Grafts undergo epidermolysis with complete loss of the epidermis and some loss of dermal cellular viability within 2 weeks after grafting, with full regeneration within 12 weeks after grafting.

Lactate dehydrogenase (viable cells = blue) of (A) a 1×2 cm normal skin sample, (B) a 3 mm full thickness biopsy of the xenograft 1 week after grafting, (C) xenografts 2 weeks after grafting with loss of viability into the mid dermis, (D) xenografts 4 weeks after grafting with partial regeneration of epidermis from the tissue edges, (E) complete regeneration of the dermis and part of the epidermis 8 weeks after grafting, and (F) complete regeneration of xenografts 12 weeks after grafting. Overview images are scanned at 4×, with inset images (identified in dashed square box) magnified. A, B, C, D, F, Representative images of five animals in each time point. E, Representative image of five animals at weeks 5 to 8 after grafting. Scale bars: 500 μm
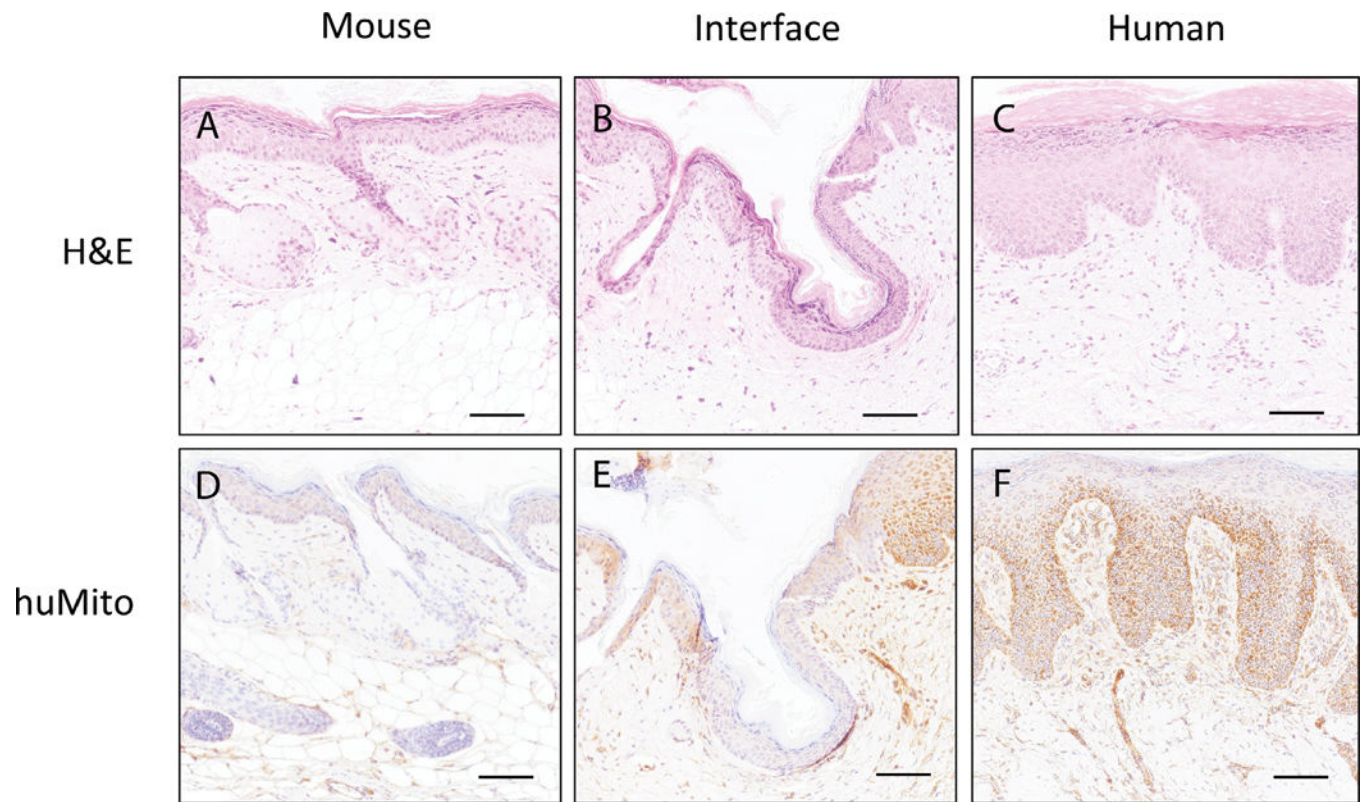
FIGURE 3. Human mitochondrial staining in human grafts 6 months after grafting reveals that the healed dermis and epidermis are human in origin.

H&E stained (A) mouse skin, (B) mouse-human skin interface, and (C) human skin graft. Human mitochondrial stained (D) mouse skin, (E) mouse-human skin interface, and (F) human skin graft; Brown = human mitochondrial antibody. Representative image of three animals. Scale bars: 100 μm
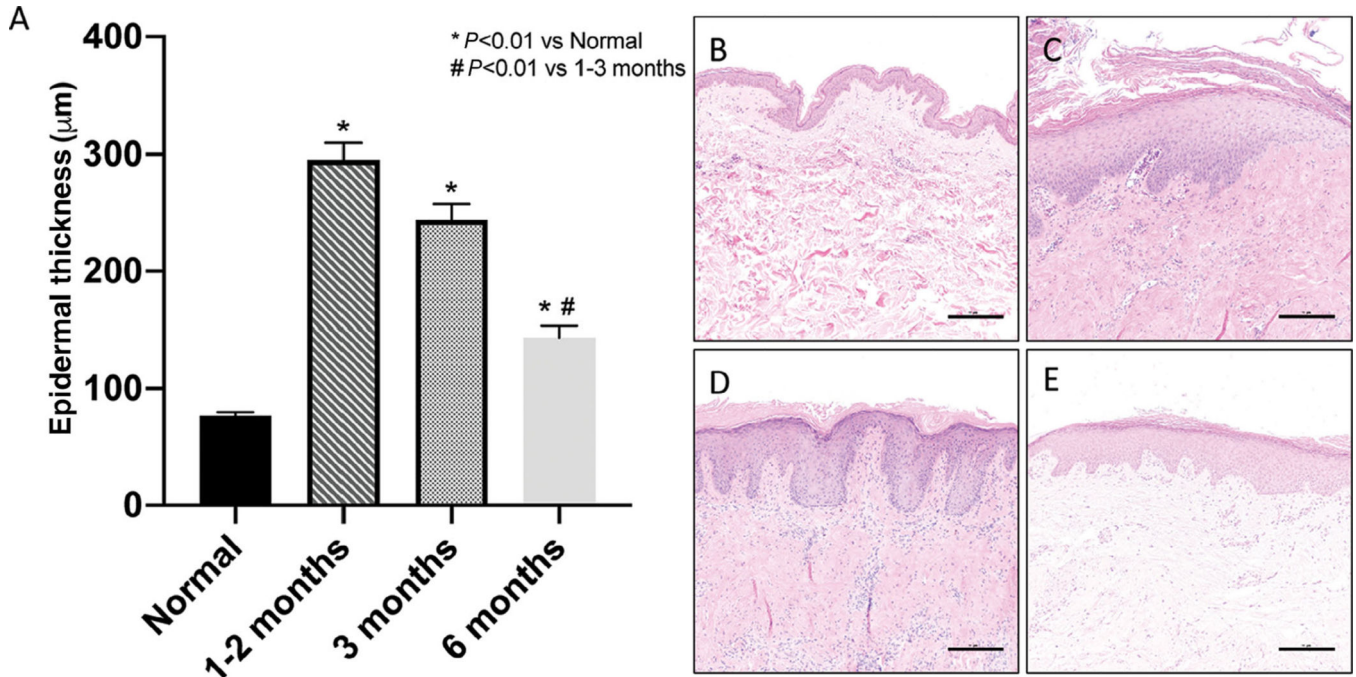
FIGURE 4. Human skin grafted onto immunocompromised mice heals with hyperproliferative epidermis that diminishes over time.

A, Quantification of epidermal thickness at baseline, 1 to 2, 3, and 6 months after grafting at various regions of the epidermis; measurements 100 μm apart along the entire width of the xenograft from three animals per timepoint. H&E stained sections of human skin at (B) time of grafting, (C) 6 weeks, (D) 12 weeks, and (E) 6 months after grafting. Representative images of three to five animals per time point. Scale bars: 500 μm
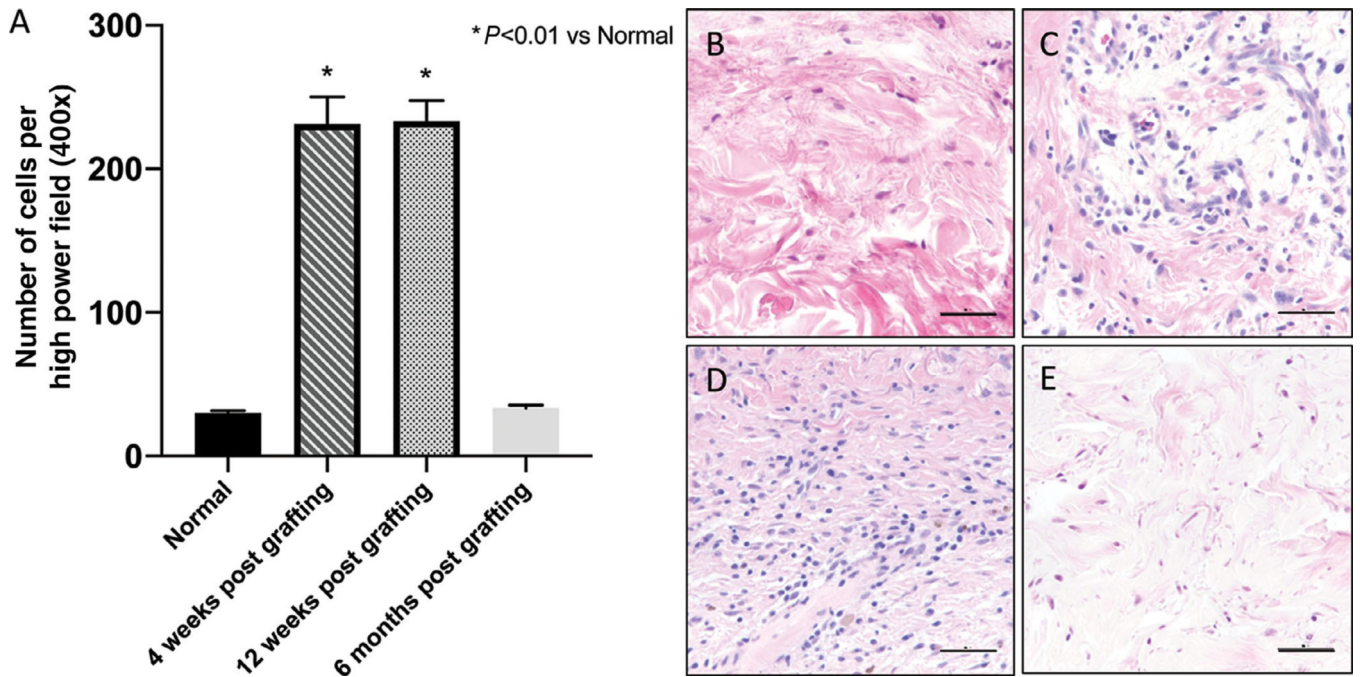
FIGURE 5. Grafts become infiltrated with non-resident immune cells in the first few months after grafting but return to baseline at 6 months post grafting.

A, Quantification of monocytes and neutrophils cells per five high power fields. B, H&E stained sections of human skin at the time of grafting, and (C) 4 weeks, (D) 12 weeks, and (E) 6 months after grafting. Representative images of three animals per timepoint. Scale bars: 50 μm
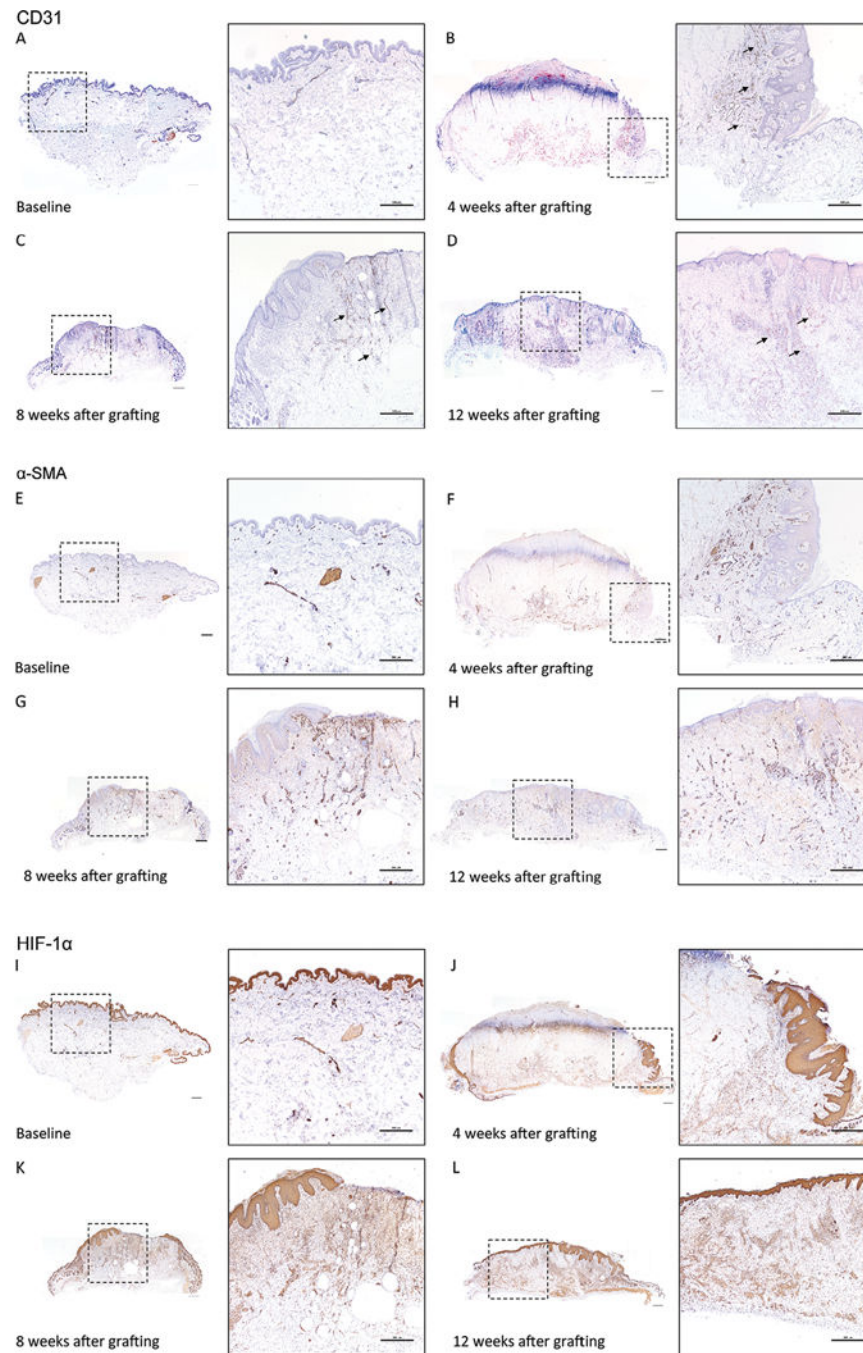
FIGURE 6. Hypoxic signal and revascularization starts from the mouse skin-human skin xenograft interface and grows inwards towards the middle of the graft.

Human CD31 staining of human skin (A) prior to grafting, and at (B) 4 weeks, (C) 8 weeks, and (D) 12 weeks after grafting. Arrows identify CD31 positive vessels. α-SMA staining of human skin (E) prior to grafting, and at (F) 4 weeks, (G) 8 weeks, and (H) 12 weeks after grafting. HIF-1α staining of human skin (I) prior to grafting, and at (J) 4 weeks, (K) 8 weeks, and (L) 12 weeks after grafting. Brown = CD31, α-SMA, HIF-1α antibody, Purple = hematoxylin. Inset boxes (dashed square box) identify the magnified regions. Representative images of three to five animals per time point. Scale bars: 500 μm
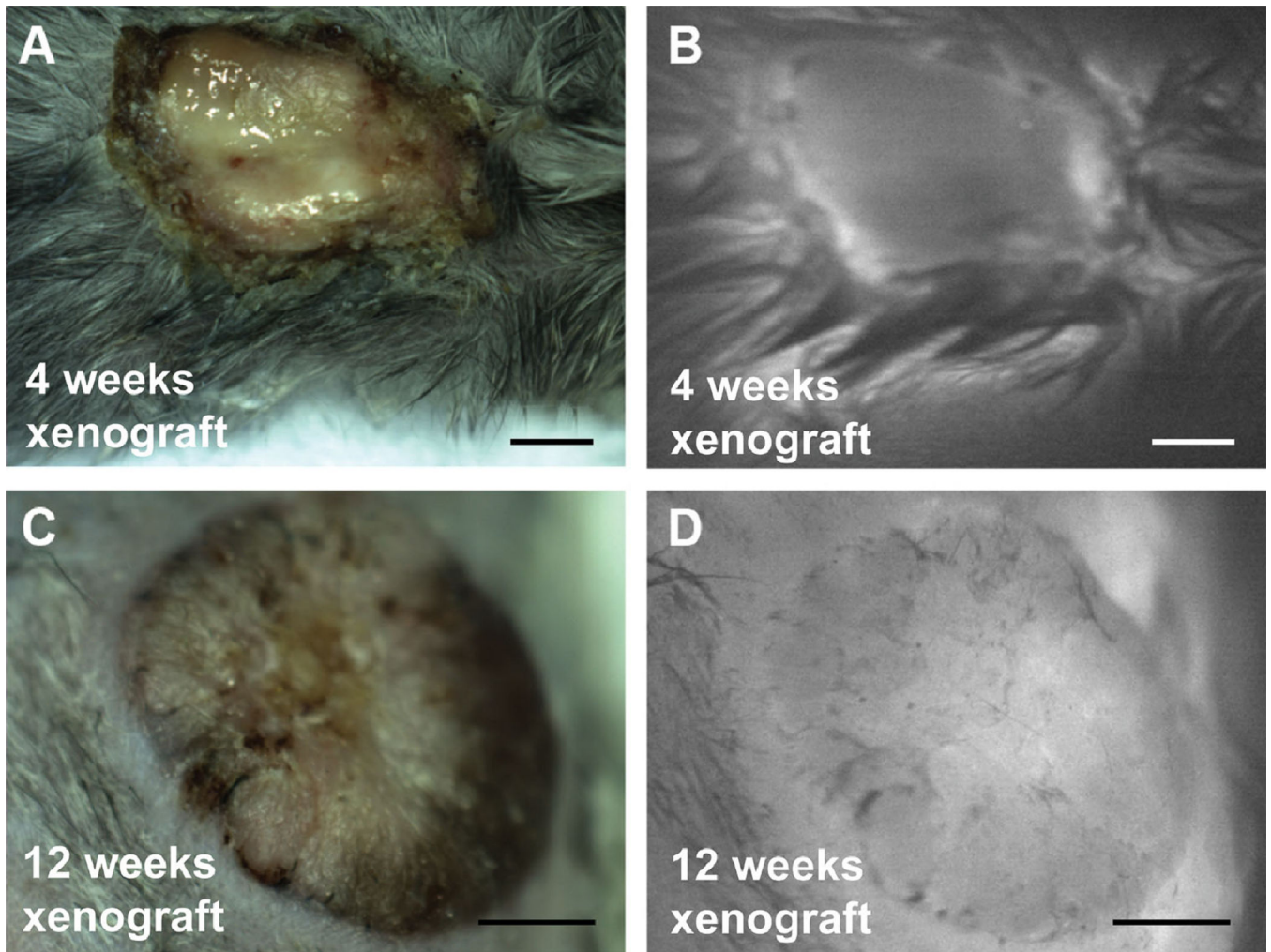
FIGURE 7. ICG fluorescence imaging demonstrates that perfusion of the xenograft increases over time after grafting.
(A) Gross white light reflectance image and (B) fluorescence image immediately after retro-orbital injection of ICG of mice with human xenografts 4 weeks after grafting. (C) Gross and (D) fluorescence image immediately after injection of ICG of human xenograft 12 weeks after grafting. Scale bars: 500 μm

TABLE 1

Anatomical differences in skin structures between different animal models and humans

Criteria	Rodents	Guinea Pig	Pig	Human
Skin attachment	Loose	Loosely attached	Firmly attached	Firmly attached
Hair coat	Dense (breed exceptions, ie, nude mice)	Sparse or dense	Sparse	Sparse
Epidermis	Thin	Thick	Thick	Thick
Dermis	Thin	Thick	Thick	Thick
Panniculus carnosus	Present	Present	Absent	Absent
Eccrine glands	Absent except in paw pads	Absent	Absent	Present
Dominant mechanism of closure	Contraction	Contraction	Re-epithelialization	Re-epithelialization